nature medicine

PAI-1 mediates the antiangiogenic and profibrinolytic effects of 16K prolactin

Khalid Bajou[1,8], Stephanie Herkenne[1,8], Victor L Thijssen[2,3], Salvino D'Amico[1], Ngoc-Quynh-Nhu Nguyen[1], Ann Bouché[4,5], Sébastien Tabruyn[1], Mohammed Srahna[1], Jean-Yves Carabin[1], Olivier Nivelles[1], Cécile Paques[1], Ivo Cornelissen[4,5], Michelle Lion[1], Agnès Noel[6], Ann Gils[7], Stefan Vinckier[4,5], Paul J Declerck[7], Arjan W Griffioen[2], Mieke Dewerchin[4,5], Joseph A Martial[1,9], Peter Carmeliet[4,5,9] & Ingrid Struman[1]

The N-terminal fragment of prolactin (16K PRL) inhibits tumor growth by impairing angiogenesis, but the underlying mechanisms are unknown. Here, we found that 16K PRL binds the fibrinolytic inhibitor plasminogen activator inhibitor-1 (PAI-1), which is known to contextually promote tumor angiogenesis and growth. Loss of PAI-1 abrogated the antitumoral and antiangiogenic effects of 16K PRL. PAI-1 bound the ternary complex PAI-1–urokinase-type plasminogen activator (uPA)–uPA receptor (uPAR), thereby exerting antiangiogenic effects. By inhibiting the antifibrinolytic activity of PAI-1, 16K PRL also protected mice against thromboembolism and promoted arterial clot lysis. Thus, by signaling through the PAI-1–uPA–uPAR complex, 16K PRL impairs tumor vascularization and growth and, by inhibiting the antifibrinolytic activity of PAI-1, promotes thrombolysis.

Angiogenesis contributes to numerous disorders, including cancer and ocular disease[1]. Studies over the last decades have identified multiple molecules regulating this process. We have previously reported that members of the prolactin (PRL) family stimulate angiogenesis, whereas their respective N-terminal peptide fragments have antiangiogenic properties[2]. Proteolytic cleavage of PRL by cathepsin D, matrix metalloproteinases or bone morphogenetic protein generates a fragment with a molecular mass of 16 kDa, named 16K PRL or vasoinhibin[3]. Although PRL has multiple physiological effects, the sole activity of 16K PRL identified to date is inhibition of angiogenesis, which has tumor growth-inhibiting effects[4–9]. 16K PRL levels are increased in retinopathy[10], preeclampsia[11] and postpartum cardiomyopathy[12,13].

The mechanisms whereby 16K PRL inhibits angiogenesis have only been partially elucidated. 16K PRL induces endothelial cell cycle arrest[14] and inhibits the activation of extracellular signal–regulated kinase (ERK1/2) induced by basic fibroblast growth factor (bFGF) or vascular endothelial growth factor (VEGF)[15,16]. In addition, 16K PRL induces endothelial cell apoptosis by activating caspase-3 and nuclear factor-κB (NF-κB)[17].

Endothelial cells express a high-affinity binding site for 16K PRL[18], but the identity of this putative 'receptor' remains elusive. Here, we identify PAI-1, which inhibits the fibrinolytic agents tissue-type plasminogen activator (tPA) and uPA[19], as a binding partner of 16K PRL, and show a functional requirement for PAI-1 in mediating the antiangiogenic and antitumor growth effects of 16K PRL. In view of the proangiogenic and prothrombotic properties of the tumor milieu, the antiangiogenic and profibrinolytic activities of 16K PRL might be attractive for antitumor therapy.

RESULTS

PAI-1 is a binding partner of 16K PRL

To identify 16K PRL binding proteins, we performed yeast two-hybrid screening. Using 16K PRL as bait and a cDNA library from primary human umbilical vein endothelial cells (HUVECs) as prey, we identified PAI-1 as the most frequently represented binding partner (~10% of all clones). Four clones contained distinct fragments of the PAI-1–encoding cDNA sequence (**Fig. 1a**). Sequence alignment identified two regions shared by at least three different clones. The location of these regions in the three-dimensional structure of PAI-1 revealed a close proximity to the reactive center loop of active PAI-1 (**Fig. 1b**).

To confirm the interaction between 16K PRL and PAI-1, we performed immunoprecipitation assays using recombinant 16K PRL and PAI-1. This analysis revealed formation of a 16K PRL–PAI-1 complex (**Fig. 1c**). 16K PRL also formed a complex with endogenous PAI-1 in the culture medium of HUVECs, as well as in human and mouse plasma (**Fig. 1c**). We confirmed the interaction between 16K PRL and PAI-1 by surface plasmon resonance analysis (SPR), which showed that 16K PRL bound to PAI-1 with a K_d of 1.1 μM (**Fig. 1d**). No binding to PAI-1 was detectable to full-length PRL (data not shown).

[1]Molecular Angiogenesis Laboratory, Interdisciplinary Cluster in Applied Genoproteomics (GIGA) Research Center, University of Liège, Liège, Belgium. [2]Angiogenesis Laboratory, Department of Medical Oncology, VU University Medical Center, Amsterdam, the Netherlands. [3]Department of Radiotherapy, VU University Medical Center, Amsterdam, the Netherlands. [4]Laboratory of Angiogenesis and Neurovascular Link, Vesalius Research Center (VRC), VIB, Leuven, Belgium. [5]Laboratory of Angiogenesis & Neurovascular Link, Department of Oncology, KU Leuven, Leuven, Belgium. [6]Unit of Biology of Tumor and Development, GIGA Research Center, University of Liège, Liège, Belgium. [7]Laboratory for Therapeutic and Diagnostic Antibodies, Department of Pharmaceutical and Pharmacological Sciences, KU Leuven, Leuven, Belgium. [8]These authors contributed equally to this work. [9]These authors jointly supervised this work. Correspondence should be addressed to I.S. (i.struman@ulg.ac.be).

Received 17 December 2013; accepted 9 April 2014; published online 15 June 2014; doi:10.1038/nm.3552

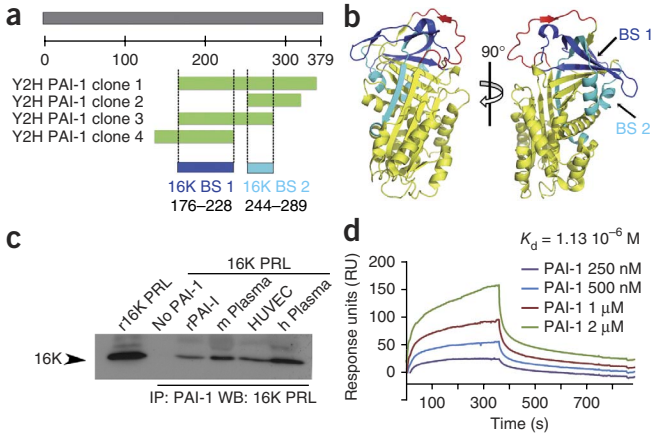

Figure 1 16K PRL interacts with PAI-1. (**a**) Sequence alignment (block presentation) of four PAI-1 clones (clone 1, K176/V364; clone 2, E244/E313; clone 3, G174/K289; clone 4, W140/P228; green bars) isolated in a yeast two-hybrid screen (Y2H) for 16K PRL binding partners, containing distinct fragments of the PAI-1 sequence (gray bar). The alignment identified two regions, 16K BS1 and 16K BS2 (blue bars), shared by at least three different clones, comprising the amino acid residues indicated. (**b**) Ribbon representation of native PAI-1 (Protein Data Bank no. 1DB2; ref. 44) showing the location of the putative binding sites for 16K PRL. Regions corresponding to 16K BS1 (dark blue) and 16K BS2 (light blue) close to the reactive center loop (red) are indicated. The structure on the right shows a 90° rotated view. (**c**) Western blot (WB) detection of 16K PRL after immunoprecipitation (IP) of recombinant human PAI-1 (rPAI-1) or endogenous PAI-1 from HUVEC-conditioned medium or human (h) or mouse (m) plasma. Input was recombinant 16K PRL (r16K PRL). Lanes 2 and 3 show a negative and positive control in the absence or presence of rPAI-1, respectively. (**d**) Representative dose-response surface plasmon resonance sensorgrams of binding of PAI-1 (250 nM, 500 nM, 1 µM and 2 µM) to immobilized 16K PRL.

Inhibition of tumor growth by 16K PRL is PAI-1 dependent

To determine whether PAI-1 is required for the antitumor activity of 16K PRL, we analyzed tumor progression of mouse B16F10 melanoma cells in wild-type (WT) mice and mice with genetic knockout of PAI-1 (*Serpine1*$^{-/-}$, here called PAI-1 KO) following infection with an adenovirus expressing 16K PRL (16K-Ad1)[7]. Infection resulted in comparable 16K PRL plasma levels in the two genotypes (**Fig. 2a**). PAI-1 deficiency did not reduce B16F10 tumor growth, probably because these tumors grew too rapidly, in accord with the contextual angiogenic activity of PAI-1 (ref. 20). Notably, overexpression of 16K PRL reduced tumor growth (**Fig. 2b**) and tumor cell proliferation (**Supplementary Fig. 1a**,**b**) in WT mice (in line with a previous study[7]) but not in PAI-1 KO mice. Immunostaining for the endothelial marker CD31 revealed that PAI-I deficiency or 16K PRL overexpression in WT mice reduced B16F10 tumor angiogenesis (**Fig. 2c**,**d**), although this effect did not achieve statistical significance for PAI-1 deficiency (P = 0.08), probably because of the rapid tumor growth (**Fig. 2c**,**d** and **Supplementary Fig. 1a**,**c**). The inhibition of tumor angiogenesis by 16K PRL is in agreement with previous studies[7,9]. In contrast to the antiangiogenic effect of 16K PRL treatment in WT mice, treatment of PAI-1 KO mice with 16K-Ad did not have an antiangiogenic effect (**Fig. 2c**,**d**). Immunoprecipitation experiments showed that 16K PRL formed a complex with PAI-1 in the blood and tumors of WT mice (**Fig. 2e**,**f**).

To confirm that PAI-1 is required for the antitumor activity of 16K PRL, we restored PAI-1 expression in PAI-1 KO mice using an adenoviral vector expressing human PAI-1 (PAI-1-Ad2)[21]. Human PAI-1 plasma levels in PAI-1 KO mice injected with PAI-1-Ad2 were 2.83 ± 0.48 µg/ml (mean ± s.d.), whereas human PAI-1 was undetectable in PAI-1 KO mice injected with control adenovirus (CTL-Ad2). Upon treatment with 16K-Ad1, plasma levels of 16K PRL were comparable in PAI-1 KO mice treated with PAI-1-Ad2 or CTL-Ad2 (**Fig. 2g**). Notably, expression of human PAI-1 in PAI-1 KO mice restored the antitumor effect of 16K PRL to that observed in WT mice (**Fig. 2h**).

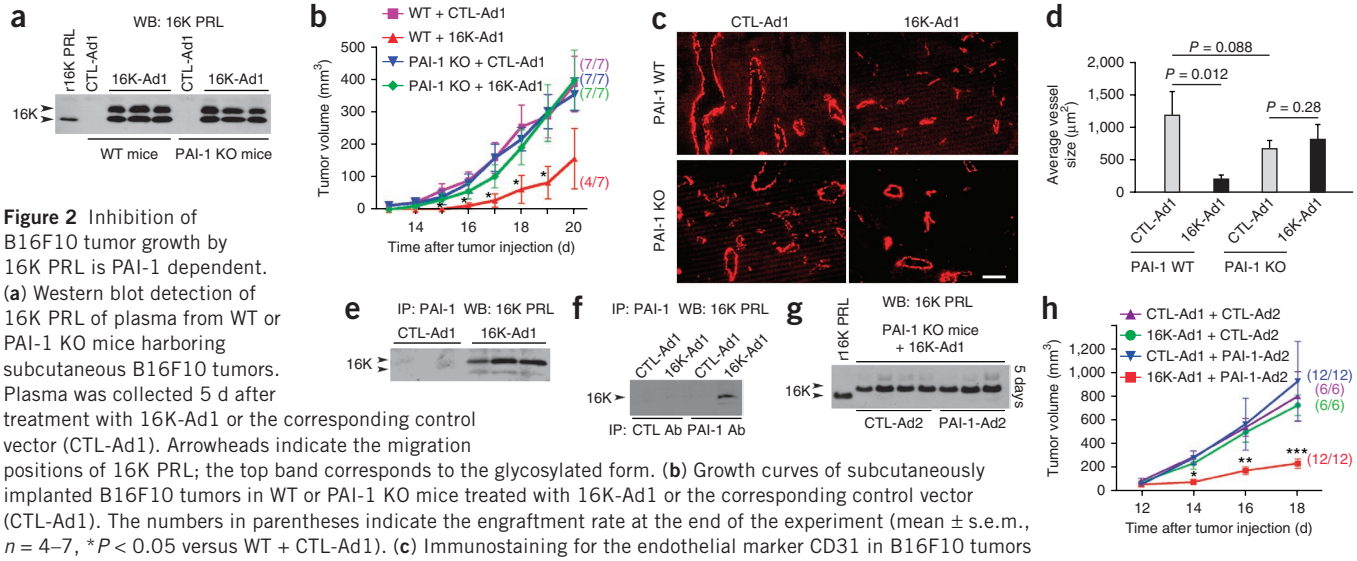

Figure 2 Inhibition of B16F10 tumor growth by 16K PRL is PAI-1 dependent. (**a**) Western blot detection of 16K PRL of plasma from WT or PAI-1 KO mice harboring subcutaneous B16F10 tumors. Plasma was collected 5 d after treatment with 16K-Ad1 or the corresponding control vector (CTL-Ad1). Arrowheads indicate the migration positions of 16K PRL; the top band corresponds to the glycosylated form. (**b**) Growth curves of subcutaneously implanted B16F10 tumors in WT or PAI-1 KO mice treated with 16K-Ad1 or the corresponding control vector (CTL-Ad1). The numbers in parentheses indicate the engraftment rate at the end of the experiment (mean ± s.e.m., n = 4–7, *P < 0.05 versus WT + CTL-Ad1). (**c**) Immunostaining for the endothelial marker CD31 in B16F10 tumors grown in WT or PAI-1 KO mice treated with 16K-Ad1 or CTL-Ad1. Scale bar, 250 µm. (**d**) Quantification of tumor vessel size in tumors of mice in **c** (mean ± s.e.m., n = 4–7). (**e**,**f**) Western blot detection of 16K PRL after immunoprecipitation of endogenous PAI-1 from plasma (**e**) or from extracts of B16F10 tumors (**f**) of mice treated with 16K-Ad1 or CTL-Ad1. Ab, antibody. (**g**) Western blot detection of 16K PRL of plasma from PAI-1 KO mice harboring subcutaneous B16F10 tumors. Plasma was collected 5 d after treatment with 16K-Ad1 and either PAI-1-Ad2 or CTL-Ad2. (**h**) Growth curves of subcutaneously implanted B16F10 tumors in PAI-1 KO mice treated with 16K-Ad1, PAI-1-Ad2 or their corresponding control vectors. The numbers in parentheses indicate the engraftment rate at the end of the experiment (mean ± s.e.m., n = 6–12, *P = 0.006, **P = 0.0006, ***P = 0.0001 versus CTL-Ad1 + CTL-Ad2).

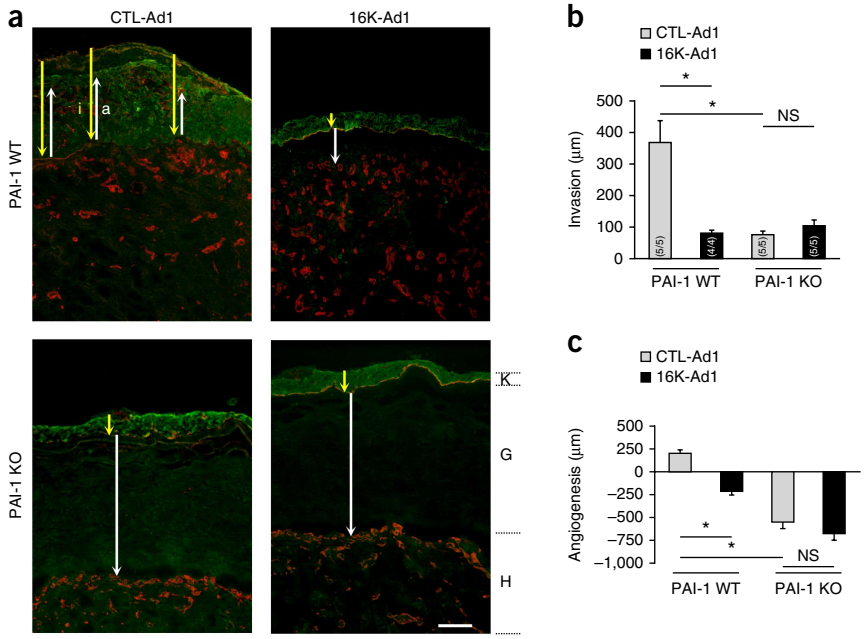

Figure 3 Inhibition of keratinocyte tumor growth by 16K PRL is PAI-1 dependent. (**a**–**c**) Tumor cell invasion and angiogenesis using the malignant mouse BD VII keratinocyte transplantation chamber model. The chamber was implanted in the skin of WT and PAI-1 KO mice treated with 16K-Ad1 or CTL-Ad1. (**a**) Representative micrographs of transversal sections of the transplants. Tumor cells were visualized by staining for antibody to keratin (green) and blood vessels by staining for antibody to collagen IV (red) at 2 weeks after transplantation. K, keratinocytes; G, collagen gel; H, host connective tissue; i, invasion parameter (distance from top of tumor cell layer to deepest invasion front, as denoted by yellow arrows); a, angiogenesis parameter (white arrows, distance over which host vessels grew into the tumor (left top) or distance between tumor cells and front of ingrowing host vessels (other micrographs). Scale bar, 100 μm. (**b**,**c**) Quantification of tumor invasion (distance i, yellow arrows in **a**) (**b**) and angiogenesis (distance a, white arrows in **a**) (**c**). Values for angiogenesis are negative when vessels do not reach the tumor tissue; in this case, the value is the distance between the tumor cells and the front of ingrowing host vessels. In **b**, the numbers in the bars indicate the engraftment rate (mean ± s.e.m.; $n = 4$ or 5, $^*P < 0.001$). NS, not significant.

We confirmed these results in another orthotopic tumor model using mouse 4T1 breast tumor cells (**Supplementary Fig. 1d**). Thus, PAI-1 is required for the antitumor effect of 16K PRL.

We also used a tumor model that is dependent on host PAI-1 (refs. 22–24). PAI-1 deficiency impairs invasion and vascularization of mouse malignant keratinocytes orthotopically transplanted in a collagen gel onto the skin[22]. Transplantation of these keratinocytes induces a stromal response, whereby host vessels and granulation tissue grow into and replace the collagen gel, through which keratinocytes invade the underlying stroma. In agreement with previous findings[23], PAI-1 deficiency substantially reduced tumor cell invasion and vascularization in this model (**Fig. 3a**–**c**). Whereas 16K-Ad1 treatment of WT mice impaired tumor cell invasion and vascularization (**Fig. 3a**), 16K PRL treatment did not further impede tumor cell invasion and vascularization in PAI-1 KO mice (**Fig. 3a**–**c**).

PAI-1 is required for 16K PRL's antiangiogenic activity

We further studied the role of PAI-1 in mediating the antiangiogenic effect of 16K PRL. We first investigated the effect of 16K PRL on retinal vascular growth. The mouse retina is avascular at birth, but blood vessels progressively sprout from the center toward the periphery during the first days after birth[25]. Compared to WT neonates, radial extension of the vascular plexus was reduced in PAI-1 KO newborns at postnatal day 4.5, indicating impaired vessel sprouting (**Fig. 4a**,**b**). Intraocular injection of recombinant 16K PRL impeded vessel sprouting in WT pups but not in PAI-1 KO pups (**Fig. 4a**,**b**).

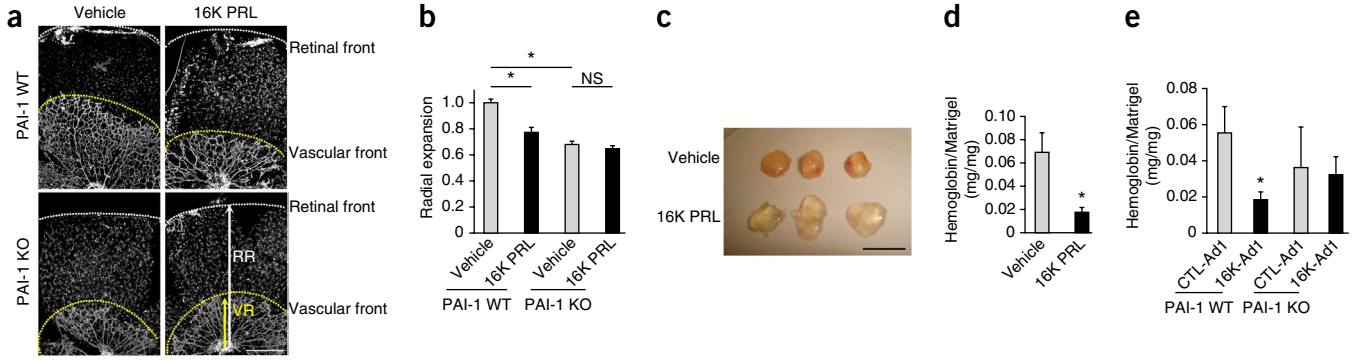

Figure 4 PAI-1 is required for 16K PRL to impair neovascularization. (**a**) Isolectin-B4 staining of flat-mounted retinas from postnatal day 4.5 WT and PAI-1 KO neonates upon treatment with vehicle or recombinant 16K PRL by intravitreal injection at postnatal day 1. The retinal radius (from the optic nerve to the edge of the retina, RR (white arrow)) and the vascular radius (from the optic nerve to the vascular front, VR (yellow arrow)) were used to calculate the radial expansion of the retinal vascular plexus. Scale bar, 500 μm. (**b**) Quantification of the radial expansion of the retinal vascular plexus calculated as ratio between VR and RR. Data are expressed relative to WT mice treated with vehicle (mean ± s.e.m.; $n = 8$–10 eyes; $^*P < 0.001$ versus vehicle-treated PAI-1 WT mice). (**c**,**d**) Photographs (**c**) and hemoglobin content (**d**) of Matrigel plugs 7 d after implantation of Matrigel mixed with vehicle or recombinant 16K PRL into WT mice (mean ± s.e.m., $n = 10$, $^*P = 0.017$). Scale bar, 1 cm. (**e**) Hemoglobin content of Matrigel plugs implanted into WT or PAI-1 KO mice treated with 16K PRL adenovirus (16K-Ad1) or control vector (CTL-Ad1) (mean ± s.e.m.; $n = 6$–8, $^*P = 0.027$ versus corresponding CTL-Ad1 treatment).

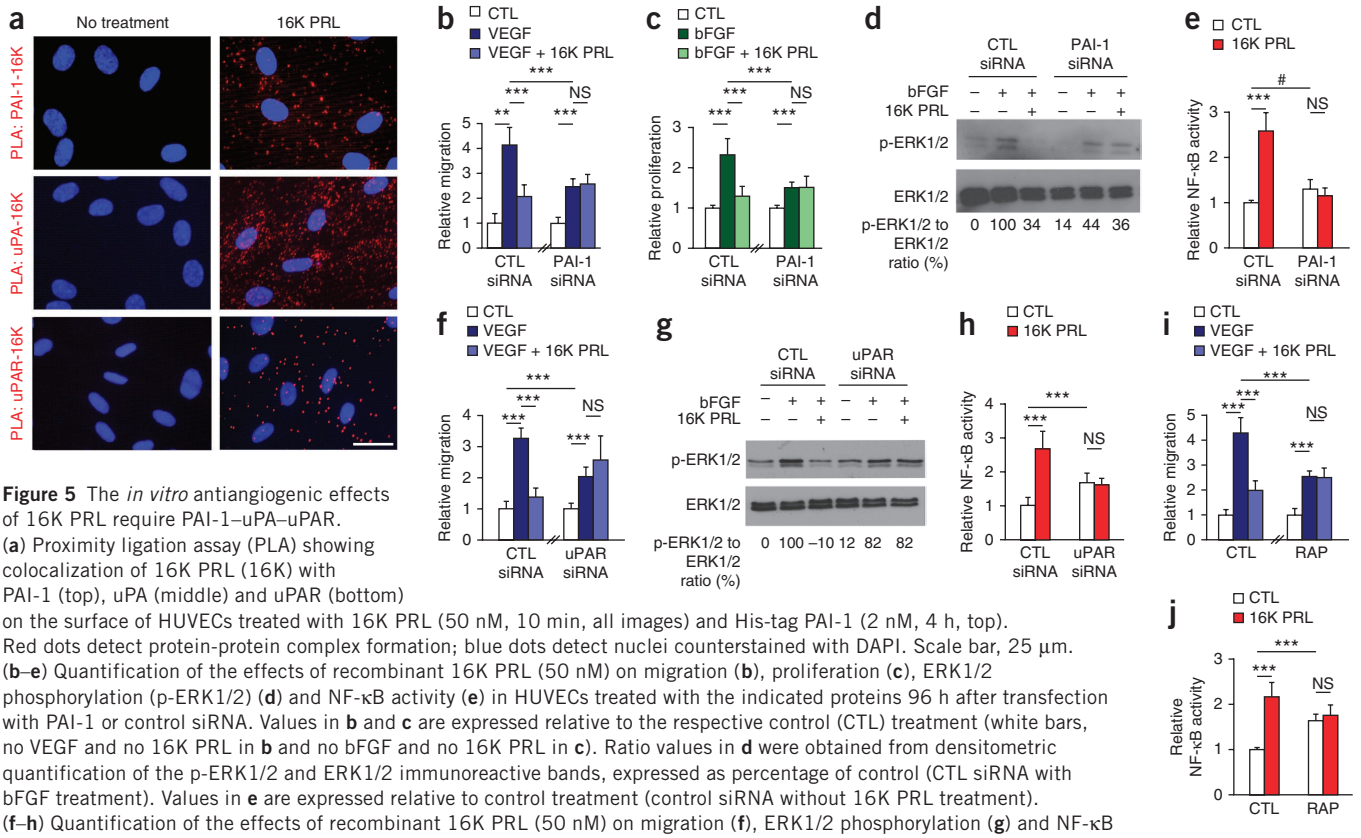

Figure 5 The *in vitro* antiangiogenic effects of 16K PRL require PAI-1–uPA–uPAR. (**a**) Proximity ligation assay (PLA) showing colocalization of 16K PRL (16K) with PAI-1 (top), uPA (middle) and uPAR (bottom) on the surface of HUVECs treated with 16K PRL (50 nM, 10 min, all images) and His-tag PAI-1 (2 nM, 4 h, top). Red dots detect protein-protein complex formation; blue dots detect nuclei counterstained with DAPI. Scale bar, 25 μm. (**b**–**e**) Quantification of the effects of recombinant 16K PRL (50 nM) on migration (**b**), proliferation (**c**), ERK1/2 phosphorylation (p-ERK1/2) (**d**) and NF-κB activity (**e**) in HUVECs treated with the indicated proteins 96 h after transfection with PAI-1 or control siRNA. Values in **b** and **c** are expressed relative to the respective control (CTL) treatment (white bars, no VEGF and no 16K PRL in **b** and no bFGF and no 16K PRL in **c**). Ratio values in **d** were obtained from densitometric quantification of the p-ERK1/2 and ERK1/2 immunoreactive bands, expressed as percentage of control (CTL siRNA with bFGF treatment). Values in **e** are expressed relative to control treatment (control siRNA without 16K PRL treatment). (**f**–**h**) Quantification of the effects of recombinant 16K PRL (50 nM) on migration (**f**), ERK1/2 phosphorylation (**g**) and NF-κB activity (**h**) in HUVECs treated with the indicated proteins 96 h after transfection uPAR siRNA. Values in **f** are expressed relative to the respective control treatment (white bars, no VEGF and no 16K PRL). Ratio values in **g** were obtained from densitometric quantification of the p-ERK1/2 and ERK1/2 immunoreactive bands, expressed as percentage of control (CTL siRNA with bFGF treatment). Values in **h** are expressed relative to control treatment (control siRNA without 16K PRL treatment). (**i**,**j**) Quantification of the effects of recombinant 16K PRL (50 nM) on migration (**i**) and NF-κB activity (**j**) in HUVECs treated with the indicated proteins together with RAP (10 nM) or control (CTL) treatment (without RAP). Values in **i** are expressed relative to the respective control treatment (white bars, no VEGF and no 16K PRL). Values in **j** are expressed relative to control treatment (no 16K PRL and no RAP). Quantitative data in **b**, **c**, **e**, **f** and **h**–**j** are descriptive means ± s.e.m. by univariate analysis of the data from three independent experiments; $^{*}P < 0.05$, $^{**}P < 0.01$, $^{***}P < 0.001$, $^{\#}P = 0.078$ versus negative or positive controls as indicated.

We also analyzed the antiangiogenic effect of 16K PRL in the Matrigel plug assay, a model that is sensitive to host PAI-1 levels (**Supplementary Fig. 1e**). Vessel ingrowth into Matrigel plugs (assayed by measuring hemoglobin content[26]) was reduced in PAI-1 KO mice, as previously reported[26], but this difference became statistically significant only after 15 d ($P < 0.001$, **Supplementary Fig. 1e**). We therefore took advantage of the intermediate reduction of Matrigel vascularization in PAI-1 KO mice at 7 d to explore whether 16K PRL would further reduce vessel ingrowth in the absence of PAI-1. Inclusion of recombinant 16K PRL in the Matrigel plug or 16K-Ad1 treatment of mice reduced Matrigel vascularization in WT but not in PAI-1 KO mice (**Fig. 4c**–**e**). Taken together, these data from various *in vivo* assays show that 16K PRL requires PAI-1 to reduce vessel growth.

16K PRL binds to a PAI-1–uPA–uPAR complex

To date, a cell surface receptor for PAI-1 has not been described, but PAI-1 is known to form a three-component cell surface complex with uPA and uPAR[27]. To investigate the role of this complex in 16K PRL's function, we first performed *in vitro* studies using HUVECs. In order to demonstrate a molecular interaction between PAI-1 and 16K PRL, we performed proximity ligation assays (PLAs) (the methods are detailed in **Supplementary Fig. 2**) using nonpermeabilized cells. In order to visualize only exogenous complexes, we performed PLA after treatment with recombinant 16K PRL and His-tagged PAI-1. As indicated by the presence of red fluorescent dots in the cells, PAI-1 and 16K PRL were located within a distance of less than 40 nm from each other (**Fig. 5a**). Notably, uPA and uPAR also colocalized with 16K PRL on the cell surface (**Fig. 5a**).

Immunoprecipitation experiments revealed the formation of PAI-1–16K PRL and uPAR–16K PRL complexes in extracts of HUVECs (**Supplementary Fig. 3a**,**b**), as well as in extracts of tumors from mice injected with 16K PRL adenovirus (**Fig. 2f** and **Supplementary Fig. 3c**). Additional SPR analysis showed that 16K PRL has a twofold higher affinity for uPA-bound PAI-1 than for PAI-1 alone: the K_d was 1.1 μM for PAI-1–16K PRL (**Fig. 1d**) and 0.5 μM for uPA–PAI-1–16K PRL (**Supplementary Fig. 3d**,**e**). Thus, 16K PRL binds to a PAI-1–uPA–uPAR complex on the surface of endothelial cells.

Inhibition of PAI-1 or uPAR abrogates the effect of 16K PRL

To investigate whether PAI-1, uPA and uPAR are required for the effects of 16K PRL on endothelial cells, we silenced or pharmacologically blocked PAI-1 and uPAR signaling. As uPAR interacts with its co-receptor lipoprotein receptor–related protein (LRP), we used treatment with recombinant receptor-associated protein (RAP), which blocks binding of uPAR to LRP[28], as a method to inhibit uPAR function. 16K PRL has a broad range of effects on endothelial cells, such as inhibition of migration[29], cell cycle arrest via inhibition

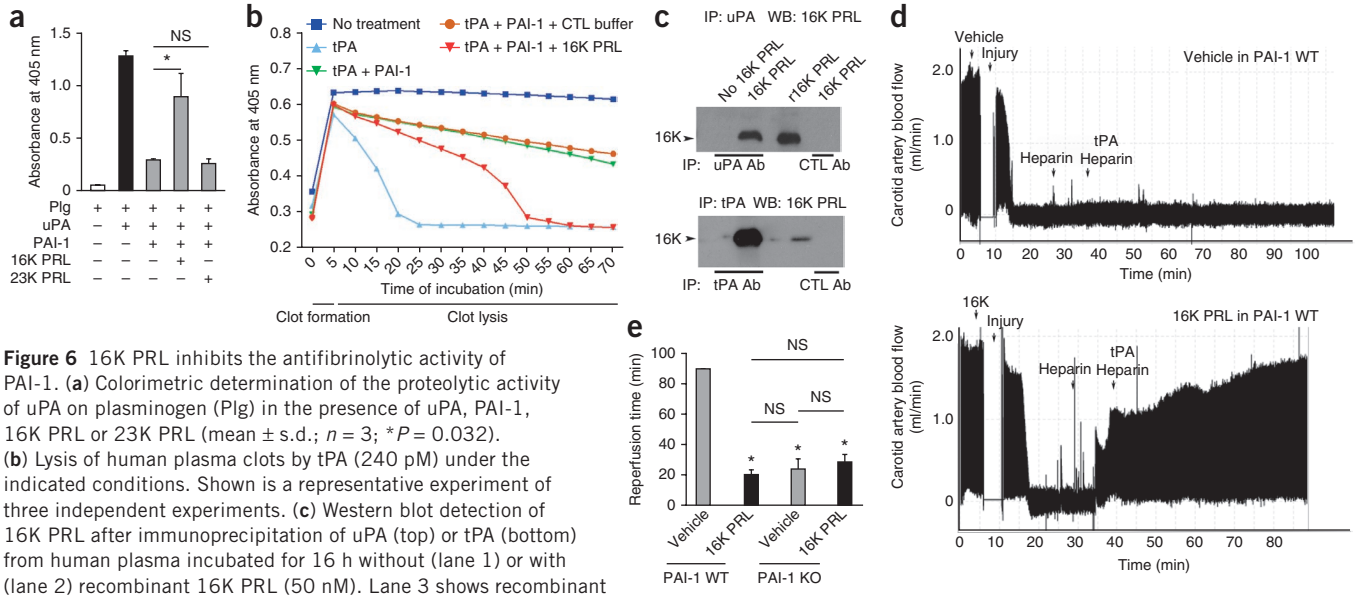

Figure 6 16K PRL inhibits the antifibrinolytic activity of PAI-1. (**a**) Colorimetric determination of the proteolytic activity of uPA on plasminogen (Plg) in the presence of uPA, PAI-1, 16K PRL or 23K PRL (mean ± s.d.; $n = 3$; $^*P = 0.032$). (**b**) Lysis of human plasma clots by tPA (240 pM) under the indicated conditions. Shown is a representative experiment of three independent experiments. (**c**) Western blot detection of 16K PRL after immunoprecipitation of uPA (top) or tPA (bottom) from human plasma incubated for 16 h without (lane 1) or with (lane 2) recombinant 16K PRL (50 nM). Lane 3 shows recombinant 16K PRL as a positive control; lane 4 shows negative controls using mouse IgG as the immunoprecipitation control antibody. (**d**) A representative blood flow recording (Doppler) from a blood flow restoration model in which the carotid artery is injured. Five minutes before carotid injury, vehicle (top) or 16K PRL (1.5 mg per kg body weight) (bottom) was administered. Ten minutes after ferric chloride injury–mediated occlusion, a bolus of unfractionated porcine heparin (200 U per kg body weight) was administered followed by a continuous heparin infusion (70 U per kg body weight per h). Ten minutes later, a continuous tPA infusion (100 μg per kg body weight per min) was started. (**e**) Reperfusion time calculated as the time interval between tPA administration and blood flow restoration (return of carotid flow to 50% of baseline). A time value of 90 min was used for conditions under which no restoration of blood flow was observed. Values in **e** are mean ± s.e.m.; $n = 6$, $^*P < 0.001$ versus vehicle in WT mice by Student's *t*-test.

of ERK1/2 phosphorylation[14–16] and induction of apoptosis via NF-κB activation[17,30]. siRNA-mediated silencing of PAI-1 by 70% (**Supplementary Fig. 4a**,**b**) or of uPAR by 78% (**Supplementary Fig. 4c**), or treatment with recombinant RAP reduced endothelial cell migration, proliferation and ERK1/2 phosphorylation in response to VEGF or bFGF and increased NF-κB activation (**Fig. 5b**–**j**). Moreover, neutralization of either PAI-1 or uPAR abrogated the effect of 16K PRL on these endothelial cell responses (**Fig. 5b**–**j**). These results indicate that PAI-1 and uPAR regulate endothelial cell responses *in vitro* and are required for the effects of 16K PRL. Notably, tumor growth in uPA-deficient mice was not affected by treatment with 16K-Ad1, indicating that uPA is required to mediate the antitumor activity of 16K PRL *in vivo* (**Supplementary Fig. 5a**). Thus, a PAI-1–uPA–uPAR complex (schematically illustrated in **Supplementary Fig. 5b**) is required for 16K PRL to impair angiogenesis.

16K PRL impairs the uPA inhibitory activity of PAI-1

Having shown that PAI-1 is necessary for 16K PRL to impair vascularization, we explored whether this peptide also interferes with other functions of PAI-1, focusing on its inhibitory effect on fibrinolysis. We found that 16K PRL reduced the ability of PAI-1 to inhibit the proteolytic activation of plasminogen by uPA, whereas full-length PRL did not have this effect (**Fig. 6a**).

For 16K PRL to be capable of inhibiting plasma PAI-1 and thereby affecting clot lysis, this peptide would need to be able to bind to the different forms of PAI-1 in the circulation. Addition of vitronectin, which forms a complex with PAI-1 and thereby prolongs its half-life[31,32], did not prevent 16K PRL from forming a complex with PAI-1 (**Supplementary Fig. 6a**) or from inhibiting its antiproteolytic activity (**Supplementary Fig. 6b**). In the circulation, PAI-1 is also present in a latent inactive form. As revealed by immunoprecipitation and SPR assays, 16K PRL also formed complexes with latent PAI-1 (**Supplementary Fig. 6a**,**c**).

16K PRL improves fibrinolysis *in vitro* and *in vivo*

To study the effect of 16K PRL on fibrinolysis, we first tested whether 16K PRL affects blood clot dissolution using an *in vitro* fibrin clot lysis assay[33]. As expected, the thrombolytic agent tPA promoted clot lysis, and addition of recombinant PAI-1 counteracted the effects of tPA. Notably, 16K PRL reduced the antifibrinolytic effect of PAI-1 (**Fig. 6b**). Immunoprecipitation showed that 16K PRL, when added to human plasma, formed complexes with uPA or tPA (**Fig. 6c**). However, 16K PRL did not accelerate clot lysis when recombinant PAI-1 was absent (**Supplementary Fig. 7a**).

We next assessed whether 16K PRL treatment could enhance the ability of tPA to induce fibrinolysis in a mouse arterial blood flow restoration model *in vivo*. We induced a thrombus in the carotid artery by applying ferric chloride to the adventitia and monitored blood flow (**Fig. 6d**). Compared to the control group, the reperfusion time was shortened in 16K PRL–treated WT mice (**Fig. 6e** and **Supplementary Table 1**). To test the ability of 16K PRL to enhance the fibrinolytic action of tPA, we injected a suboptimal dose of tPA 20 min after vessel occlusion. Confirming previous reports[34], the reperfusion time was also shortened in PAI-1 KO mice, but 16K PRL failed to further shorten the reperfusion time in PAI-1 KO mice (**Fig. 6e** and **Supplementary Table 1**).

Lastly, we evaluated 16K PRL's ability to inhibit PAI-1 in a mouse thromboembolism model in which intravenous injection of thromboplastin induces a systemic thrombotic response and death. In survival studies, treatment of mice with recombinant 16K PRL 5 min before thromboplastin injection increased the survival rate from 27% to 68% (**Supplementary Fig. 7b**). Similarly, treatment with 16K-Ad1 5 d before thromboplastin injection increased the survival rate from 20% to 73% (**Supplementary Fig. 7c**). Histological analysis of lung sections confirmed a higher number of occluded vessels with thrombi in control mice than in 16K PRL–treated WT mice (**Supplementary Fig. 7d**). As reported[35], the survival rate was higher in PAI-1 KO

than in WT mice after thromboplastin injection (**Supplementary Fig. 7e**). However, the survival rate was not significantly improved in PAI-1 KO mice treated with 16K-Ad1 (**Supplementary Fig. 7e**). Immunoprecipitation of PAI-1 in plasma after induction of thromboembolism revealed the presence of a complex between PAI-1 and 16K PRL in WT mice injected with recombinant 16K PRL or 16K-Ad1 (**Supplementary Fig. 7e**).

DISCUSSION

In various preclinical models, 16K PRL has been reported to reduce tumor progression and metastasis through its antiangiogenic activity[4–7]. Here, we investigated the mechanisms underlying these effects and demonstrated that the antiangiogenic activity of 16K PRL relies on the formation of a complex with PAI-1. In PAI-1 KO mice, 16K PRL is no longer able to impair vascular outgrowth in physiological (retina), experimental (Matrigel) and pathological (tumor) models.

In vitro studies revealed that 16K PRL colocalizes with uPA and uPAR on the surface of endothelial cells. Using blocking antibodies or siRNA silencing, we showed that uPAR is required for the *in vitro* antiangiogenic effects of 16K PRL. By binding uPA, uPAR localizes proteolytic activity at the leading edge of invading cells[36], but this receptor also functions as a signaling hub[37,38]. As uPAR is a glycosylphosphatidylinositol-anchored membrane protein, it uses other transmembrane proteins to signal, such as LRP. Our data show that blocking LRP function using RAP (which blocks the uPAR-LRP interaction) or silencing uPAR using siRNA prevents 16K PRL's activity and signaling in endothelial cells. The observation that the affinity of 16K PRL for PAI-1 is rather weak (K_d = 1.1 μM), at least as compared to its nanomolar potency in affecting endothelial cell responses, suggests that the binding affinity of 16K PRL is higher for the natural multicomponent PAI-1–uPA–uPAR–LRP complex. Indeed, the K_d of 16K PRL increased by twofold for the PAI-1–uPA complex compared to PAI-1 alone. As we detected complexes between 16K PRL and uPAR in tumor extracts, we hypothesize that uPAR and LRP are also required for 16K PRL's full antiangiogenic activity. Notably, we found that 16K PRL bound to all forms of PAI-1 found in the circulation, including latent PAI-1, PAI-1 bound to vitronectin and PAI-1 complexed to uPA.

Several lines of evidence indicate that PAI-1 is necessary for the antiangiogenic activity of 16K PRL. First, immunoprecipitation and SPR assays showed that PAI-1 bound to 16K PRL. Second, the antitumor and antiangiogenic activity of this fragment was lost in PAI-1 KO mice, and third, these effects were restored upon re-expression of PAI-1 in these knockout mice. Fourth, recombinant 16K PRL no longer reduced angiogenesis in the retina and Matrigel assay in PAI-1 KO mice. Notably, the effect of 16K PRL in WT mice was never more potent than the effect of complete PAI-1 deficiency. This suggests that 16K PRL does not have additional effects beyond binding PAI-1, although we cannot formally exclude the possibility that 16K PRL might interact with other molecules. Overall, these genetic and pharmacological findings provide compelling evidence for a role of PAI-1 in mediating 16K PRL's biological effects.

PAI-1 is a potent inhibitor of the plasminogen activators tPA and uPA. Its presence in plasma, platelets and the vasculature determines resistance to arterial thrombolysis[34]. Identifying PAI-1 as a binding partner for 16K PRL prompted us to explore whether this interaction modulated its antiproteolytic function, particularly as the 16K PRL binding site is located near the reactive center loop of PAI-1, which is involved in the enzymatic function of PAI-1. Our data show that 16K PRL promoted fibrin clot lysis *in vitro* in the presence of exogenously added PAI-1 but failed to affect fibrinolysis in the absence of PAI-1. In WT mice *in vivo*, 16K PRL reduced the time to reperfusion in an arterial blood flow restoration model and increased survival in a model of pulmonary thromboembolism. Loss of PAI-1 similarly reduced the time to reperfusion and increased survival, consistent with previous reports that PAI-1 deficiency protects against arterial and venous thrombosis[34,35,39]. However, 16K PRL treatment did not affect fibrinolysis in PAI-1 KO mice, indicating that 16K PRL counteracts the antifibrinolytic activity of PAI-1.

Elevated levels of PAI-1 have been correlated with an increased risk of cardiovascular diseases, ischemic stroke and thromboembolism[40]. Owing to its activity as a PAI-1 antagonist, 16K PRL could potentially be used to treat thrombotic disorders. Also, as arterial and venous thromboembolisms have emerged as adverse effects of angiogenesis inhibitors[41–43], the antiangiogenic and profibrinolytic properties of 16K PRL warrant further attention for the treatment of malignancies.

METHODS

Methods and any associated references are available in the online version of the paper.

Note: Any Supplementary Information and Source Data files are available in the online version of the paper.

ACKNOWLEDGMENTS

We thank J.-M. Foidart for helpful discussions. We also thank A. Igout, O. Jacquin and M. Galleni for assisting with SPR, E. Rozet for helping with statistical analysis, R. Lijnen (Center for Molecular and Vascular Biology) for providing the PAI-1 ELISA and N. Fusenig (German Cancer Research) for providing BD VII cells. We thank the technology platforms support staff at the GIGA Research Center and P. Drion of the mouse facility (GIGA). This study was supported by the University of Liège, the Fonds pour la Recherche Industrielle et Agricole (FRIA), Belgium, the Fonds National de la Recherche Scientifique (FNRS), Belgium, the Belgian Federal Science Policy Office grant IUAP06/30 (to I.S., A.N. and P.C.), Neoangio program grant no. 616476 from the 'Service Public de Wallonie' (to I.S. and A.N.), the Belgian Foundation against Cancer, Televie, the Léon Frédéricq Fund and the Centre Anticancéreux (Liège, Belgium) and Dutch Cancer Society grants UM2008-4101 and VU2009-4358 (to V.L.T. and A.W.G.). The work of P.C. is supported by the Belgian Science Policy (IAP no. P7/03), the Leducq Network of Excellence, the Flanders Research Foundation (FWO), the Foundation against Cancer, European Research Council Advanced Research Grant EU-ERC269073 and long-term structural Methusalem funding by the Flemish Government.

AUTHOR CONTRIBUTIONS

K.B. and S.H. designed, supervised and conducted the experiments, performed *in vitro* and *in vivo* studies and statistical analyses, interpreted the data and wrote the manuscript. K.B. performed tumor studies, Matrigel plug assays and pulmonary embolism and *in vitro* studies. S.H., N.-Q.-N.N. and O.N. performed arterial thrombolysis experiments. S.H., S.T., O.N. and S.V. performed retinal angiogenesis experiments. V.L.T. and A.W.G. participated in designing the yeast two-hybrid experiments and in data interpretation. S.D. performed the SPR studies. J.-Y.C. participated in *in vitro* and *in vivo* studies. C.P. and M.L. participated in *in vitro* studies. M.S. performed immunohistochemistry staining and analysis. A.N. participated in data analysis, provided scientific suggestions and contributed to the manuscript review. A.G. and P.J.D. performed the SPR analyses and participated in experiments on PAI-1 antiproteolytic activities. A.B., I.C. and S.V. contributed to *in vivo* experiment analysis and setup. J.A.M. conceived the study and revised the manuscript. M.D. and P.C. contributed to the experimental analysis and setup and participated in writing the manuscript. I.S. conceived and designed the study, performed yeast-two-hybrid screening, coordinated the experiments and wrote the manuscript. All authors read and approved the final manuscript.

COMPETING FINANCIAL INTERESTS

The authors declare no competing financial interests.

1. Chung, A.S., Lee, J. & Ferrara, N. Targeting the tumour vasculature: insights from physiological angiogenesis. *Nat. Rev. Cancer* **10**, 505–514 (2010).
2. Struman, I. *et al.* Opposing actions of intact and N-terminal fragments of the human prolactin/growth hormone family members on angiogenesis: an efficient mechanism for the regulation of angiogenesis. *Proc. Natl. Acad. Sci. USA* **96**, 1246–1251 (1999).
3. Clapp, C., Aranda, J., Gonzalez, C., Jeziorski, M.C. & Martinez de la Escalera, G. Vasoinhibins: endogenous regulators of angiogenesis and vascular function. *Trends Endocrinol. Metab.* **17**, 301–307 (2006).
4. Bentzien, F., Struman, I., Martini, J.F., Martial, J. & Weiner, R. Expression of the antiangiogenic factor 16K hPRL in human HCT116 colon cancer cells inhibits tumor growth in Rag1$^{-/-}$ mice. *Cancer Res.* **61**, 7356–7362 (2001).
5. Kim, J. *et al.* Antitumor activity of the 16-kDa prolactin fragment in prostate cancer. *Cancer Res.* **63**, 386–393 (2003).
6. Kinet, V. *et al.* Antiangiogenic liposomal gene therapy with 16K human prolactin efficiently reduces tumor growth. *Cancer Lett.* **284**, 222–228 (2009).
7. Nguyen, N.Q. *et al.* Inhibition of tumor growth and metastasis establishment by adenovirus-mediated gene transfer delivery of the antiangiogenic factor 16K hPRL. *Mol. Ther.* **15**, 2094–2100 (2007).
8. Tabruyn, S.P. *et al.* The angiostatic 16K human prolactin overcomes endothelial cell anergy and promotes leukocyte infiltration via nuclear factor-κB activation. *Mol. Endocrinol.* **21**, 1422–1429 (2007).
9. Nguyen, N.Q. *et al.* The antiangiogenic 16K prolactin impairs functional tumor neovascularization by inhibiting vessel maturation. *PLoS ONE* **6**, e27318 (2011).
10. García, C. *et al.* Vasoinhibins prevent retinal vasopermeability associated with diabetic retinopathy in rats via protein phosphatase 2A-dependent eNOS inactivation. *J. Clin. Invest.* **118**, 2291–2300 (2008).
11. González, C. *et al.* Elevated vasoinhibins may contribute to endothelial cell dysfunction and low birth weight in preeclampsia. *Lab. Invest.* **87**, 1009–1017 (2007).
12. Hilfiker-Kleiner, D. *et al.* A cathepsin D-cleaved 16 kDa form of prolactin mediates postpartum cardiomyopathy. *Cell* **128**, 589–600 (2007).
13. Halkein, J. *et al.* MicroRNA-146a is a therapeutic target and biomarker for peripartum cardiomyopathy. *J. Clin. Invest.* **123**, 2143–2154 (2013).
14. Tabruyn, S.P., Nguyen, N.Q., Cornet, A.M., Martial, J.A. & Struman, I. The antiangiogenic factor, 16-kDa human prolactin, induces endothelial cell cycle arrest by acting at both the G0–G1 and the G2-M phases. *Mol. Endocrinol.* **19**, 1932–1942 (2005).
15. D'Angelo, G. *et al.* 16K human prolactin inhibits vascular endothelial growth factor-induced activation of Ras in capillary endothelial cells. *Mol. Endocrinol.* **13**, 692–704 (1999).
16. D'Angelo, G., Struman, I., Martial, J. & Weiner, R.I. Activation of mitogen-activated protein kinases by vascular endothelial growth factor and basic fibroblast growth factor in capillary endothelial cells is inhibited by the antiangiogenic factor 16-kDa N-terminal fragment of prolactin. *Proc. Natl. Acad. Sci. USA* **92**, 6374–6378 (1995).
17. Tabruyn, S.P. *et al.* The antiangiogenic factor 16K human prolactin induces caspase-dependent apoptosis by a mechanism that requires activation of nuclear factor-κB. *Mol. Endocrinol.* **17**, 1815–1823 (2003).
18. Clapp, C. & Weiner, R.I. A specific, high affinity, saturable binding site for the 16-kilodalton fragment of prolactin on capillary endothelial cells. *Endocrinology* **130**, 1380–1386 (1992).
19. Rijken, D.C., Wijngaards, G. & Welbergen, J. Immunological characterization of plasminogen activator activities in human tissues and body fluids. *J. Lab. Clin. Med.* **97**, 477–486 (1981).
20. Eitzman, D.T., Krauss, J.C., Shen, T., Cui, J. & Ginsburg Lack of plasminogen activator inhibitor-1 effect in a transgenic mouse model of metastatic melanoma. *Blood* **87**, 4718–4722 (1996).
21. Carmeliet, P. *et al.* Inhibitory role of plasminogen activator inhibitor-1 in arterial wound healing and neointima formation: a gene targeting and gene transfer study in mice. *Circulation* **96**, 3180–3191 (1997).
22. Bajou, K. *et al.* Absence of host plasminogen activator inhibitor 1 prevents cancer invasion and vascularization. *Nat. Med.* **4**, 923–928 (1998).
23. Bajou, K. *et al.* The plasminogen activator inhibitor PAI-1 controls *in vivo* tumor vascularization by interaction with proteases, not vitronectin. Implications for antiangiogenic strategies. *J. Cell Biol.* **152**, 777–784 (2001).
24. Bajou, K. *et al.* Host-derived plasminogen activator inhibitor-1 (PAI-1) concentration is critical for *in vivo* tumoral angiogenesis and growth. *Oncogene* **23**, 6986–6990 (2004).
25. Gerhardt, H. *et al.* VEGF guides angiogenic sprouting utilizing endothelial tip cell filopodia. *J. Cell Biol.* **161**, 1163–1177 (2003).
26. McMahon, G.A. *et al.* Plasminogen activator inhibitor-1 regulates tumor growth and angiogenesis. *J. Biol. Chem.* **276**, 33964–33968 (2001).
27. Binder, B.R., Mihaly, J. & Prager, G.W. uPAR-uPA-PAI-1 interactions and signaling: a vascular biologist's view. *Thromb. Haemost.* **97**, 336–342 (2007).
28. Conese, M. *et al.* α-2 Macroglobulin receptor/Ldl receptor-related protein(Lrp)-dependent internalization of the urokinase receptor. *J. Cell Biol.* **131**, 1609–1622 (1995).
29. Lee, S.H., Kunz, J., Lin, S.H. & Yu-Lee, L.Y. 16-kDa prolactin inhibits endothelial cell migration by down-regulating the Ras-Tiam1-Rac1-Pak1 signaling pathway. *Cancer Res.* **67**, 11045–11053 (2007).
30. Martini, J.F. *et al.* The antiangiogenic factor 16K PRL induces programmed cell death in endothelial cells by caspase activation. *Mol. Endocrinol.* **14**, 1536–1549 (2000).
31. Declerck, P.J. *et al.* Purification and characterization of a plasminogen activator inhibitor 1 binding protein from human plasma. Identification as a multimeric form of S protein (vitronectin). *J. Biol. Chem.* **263**, 15454–15461 (1988).
32. Seiffert, D. & Loskutoff, D.J. Evidence that type 1 plasminogen activator inhibitor binds to the somatomedin B domain of vitronectin. *J. Biol. Chem.* **266**, 2824–2830 (1991).
33. Mutch, N.J., Thomas, L., Moore, N.R., Lisiak, K.M. & Booth, N.A. TAFIa, PAI-1 and α-antiplasmin: complementary roles in regulating lysis of thrombi and plasma clots. *J. Thromb. Haemost.* **5**, 812–817 (2007).
34. Zhu, Y., Carmeliet, P. & Fay, W.P. Plasminogen activator inhibitor-1 is a major determinant of arterial thrombolysis resistance. *Circulation* **99**, 3050–3055 (1999).
35. Shu, E., Matsuno, H., Ishisaki, A., Kitajima, Y. & Kozawa, O. Lack of plasminogen activator inhibitor-1 enhances the preventive effect of DX-9065a, a selective factor Xa inhibitor, on venous thrombus and acute pulmonary embolism in mice. *Pathophysiol. Haemost. Thromb.* **33**, 206–213 (2003).
36. Blasi, F. Urokinase and urokinase receptor: a paracrine/autocrine system regulating cell migration and invasiveness. *Bioessays* **15**, 105–111 (1993).
37. Prager, G.W. *et al.* Urokinase mediates endothelial cell survival via induction of the X-linked inhibitor of apoptosis protein. *Blood* **113**, 1383–1390 (2009).
38. LaRusch, G.A. *et al.* Factor XII stimulates ERK1/2 and Akt through uPAR, integrins, and the EGFR to initiate angiogenesis. *Blood* **115**, 5111–5120 (2010).
39. Smith, L.H. *et al.* Pivotal role of PAI-1 in a murine model of hepatic vein thrombosis. *Blood* **107**, 132–134 (2006).
40. Tsantes, A.E. *et al.* The effect of the plasminogen activator inhibitor-1 4G/5G polymorphism on the thrombotic risk. *Thromb. Res.* **122**, 736–742 (2008).
41. Nalluri, S.R., Chu, D., Keresztes, R., Zhu, X. & Wu, S. Risk of venous thromboembolism with the angiogenesis inhibitor bevacizumab in cancer patients: a meta-analysis. *J. Am. Med. Assoc.* **300**, 2277–2285 (2008).
42. Scappaticci, F.A. *et al.* Arterial thromboembolic events in patients with metastatic carcinoma treated with chemotherapy and bevacizumab. *J. Natl. Cancer Inst.* **99**, 1232–1239 (2007).
43. Zangari, M. *et al.* Thrombotic events in patients with cancer receiving antiangiogenesis agents. *J. Clin. Oncol.* **27**, 4865–4873 (2009).
44. Nar, H. *et al.* Plasminogen activator inhibitor 1. Structure of the native serpin, comparison to its other conformers and implications for serpin inactivation. *J. Mol. Biol.* **297**, 683–695 (2000).

ONLINE METHODS

Materials. Recombinant human 16K PRL was produced and purified from *Escherichia coli* as previously described[2,17]. The purity of the recombinant protein exceeded 95% (as estimated by Coomassie blue staining, data not shown). Recombinant human PAI-1 was produced in our laboratory[45]; uPA and RAP were from Calbiochem, tPA for *in vitro* experiments and plasminogen was from Sigma-Aldrich; rt-PA (Actilyse, recombinant tPA) for *in vivo* experiments was from Boehringer Ingelheim.

His-tagged PAI-1 production. In order to detect added PAI-1 in cultured cells, recombinant human PAI-1 harboring a His-tag was produced. A PAI-1–encoding cDNA was inserted into the pCold IV plasmid (Takara Bio) between restriction sites *Nde*1 and *Bam*H1. Production of His-tag PAI-1 was carried out as recommended by the manufacturer at 15 °C using One Shot BL21 Star (DE3) *E. coli* cells (Invitrogen). After cell disruption, His-tag PAI-1 was purified using a 5 ml Ni^{2+}-charged HiTrap Chelating HP column (GE Healthcare) on an AKTA Explorer Purification Unit (GE Healthcare). Approximately 50 mg of purified recombinant protein was obtained from 1 l of culture medium.

Yeast two-hybrid screening. Yeast two-hybrid screening was performed with the MATCHMAKER GAL4 Two-Hybrid System 3 (Clontech) using an approach similar to that previously used to identify galectin-1 as the binding partner for another angiogenic inhibitor, anginex[46]. Human 16K PRL–encoding cDNA (stop140, the first 139 amino acids from hPRL[17]) was used as bait and cloned into the pGBKT7 vector in frame with the GAL4 DNA-binding domain (pBD16K). The construct was tested for the absence of transcriptional activation and toxicity. Yeast AH109 cells were then co-transformed with pBD16K, *Sma*I-linearized prey vector (pGADT7) and a SMART-cDNA library generated from activated HUVEC mRNA (incubated for 24 h with bFGF (10 ng/ml), VEGF (50 ng/ml)). The cloning of the cDNA library in the prey pGADT7 vector takes place *in vivo* via homologous recombination. Following growth on agar plates of medium selective for reporter gene activation, prey plasmids from positive yeast colonies were isolated on CHROMA SPIN-1000 columns (Clontech) and shuttled into *E. coli*. Interaction was confirmed by targeted transformation of the specific constructs using the small-scale yeast transformation protocol, as described in the Yeast Protocol Handbook (Clontech). These specific constructs were full-length human PAI-1 cloned into pGADT7, pBD16K and clones isolated from the screen.

Label-free interaction analysis by surface plasmon resonance. Real-time monitoring of molecular interactions was performed at 25 °C using the BIAcore 3000 system (GE Healthcare) according to the manufacturer's instructions. Recombinant 16K PRL was immobilized to a CM5 sensor chip (BIAcore) via primary amine groups using the Amine Coupling Kit (BIAcore). 3429 RU of 16K PRL were immobilized to a flow cell of the CM5 sensor chip and 2951 RU of a control antibody to another flow cell. PAI-1, latent PAI-1 (obtained by incubating PAI-1 for 24 h at 37 °C) and PAI-1–uPA (obtained by incubating equimolar amounts of uPA and PAI-1 for 10 min at 37 °C) were injected for 360 s (30 µl/min) followed by 360 s of dissociation at the following concentrations: 250 nM, 500 nM, 1 µM and 2 µM. Association rate (*ka*) and dissociation rate (*kd*) constants were obtained by analysis of the sensorgrams using the BIAevaluation software, version 3.2. Equilibrium dissociation constant K_d is calculated from the ratio *kd*/*ka*; all measurements were performed in duplicate at all concentrations indicated.

Cell culture. All cells were cultured at 37 °C in a 5% CO_2 humid atmosphere. HUVECs were isolated as previously described[47] and maintained in EGM2 medium (Cambrex Bio Science) supplemented with 10% FCS and 100 U ml^{-1} penicillin-streptomycin. HUVECs were then cultured in medium containing 75% human endothelial serum free medium (SFM) (Invitrogen) and 25% EGM-2 (Cambrex Bio Science). Angiogenic assays were performed in SFM (Invitrogen) supplemented with bFGF (5 ng/ml). B16F10 mouse melanoma cells were obtained from the American Type Culture Collection (ATCC CRL-6475) and cultured in high-glucose DMEM supplemented with 10% FCS, 4 mM glutamine and 100 U ml^{-1} penicillin-streptomycin. 4T1 breast cancer cells (ATCC, CRL2939) were maintained in RPMI 1640 supplemented with 10% FBS, 4 mM glutamine and 100 U ml^{-1} penicillin-streptomycin. Malignant mouse keratinocytes (BD VII cells provided by N. Fusenig, German Cancer Research, Heidelberg, Germany)[48] were routinely grown in DMEM supplemented with 10% FCS and 100 U ml^{-1} penicillin-streptomycin.

Western blot analysis. Cell lysates, samples from co-immunoprecipitation experiments or mouse plasma were separated by SDS-PAGE (15% and 10%) and transferred to a polyvinylidene fluoride membrane (Millipore). Blots were blocked overnight with 5% milk in Tris-buffered saline with 0.1% Tween 20 and probed for 1 h at room temperature with primary antibodies: rabbit polyclonal anti-hPRL with the ability to recognize 16K PRL (DAKO, catalog #A0569), goat polyclonal anti-mouse uPAR (R&D Systems, catalog #AF534), rabbit polyclonal anti-human ERK1/2 (Millipore, catalog #06-182), rabbit polyclonal anti-human p-ERK1/2 (Thr202/Tyr204) (Cell Signaling, catalog #9101), mouse monoclonal anti-PAI-1 antibody (MA-33H1F7 (in-house developed, P.J.D.) and rabbit monoclonal anti-human uPAR (Cell Signaling, catalog #12713). GAPDH-HRP (Abcam, catalog #AB 9385, 1/4,000) and β-tubulin (Abcam, catalog #AB 6046, 1/4,000) loading control antibodies were used for normalization. All primary antibodies were diluted 1/1,000. After three washes with Tris-buffered saline containing 0.1% Tween 20, antigen-antibody complexes were detected with horseradish peroxidase–conjugated goat anti-rabbit (Cell Signaling, catalog #7074, 1/2,000) or rabbit anti-goat secondary (DAKO, catalog #PO449, 1/2,000) antibody and an enhanced fluoro-chemiluminescent system (ECL; Pierce). Densitometry was performed using ImageJ software.

siRNA transfections. Cells were transfected (250,000 cells per well in 6-well plates) with calcium phosphate transfection reagent. Briefly, HUVECs were transfected with PAI-1 siRNA (50 nM), uPAR siRNA (10 nM) or a control siRNA in medium containing 75% SFM (Invitrogen) and 25% EGM-2 (Cambrex Bio Science). 16 h after transfection, HUVECs were collected and seeded for further assays in SFM supplemented with bFGF (5 ng/ml). Assays were performed after 96 h of transfection for PAI-1 silencing and 72 h for uPAR silencing. The sequences of the PAI-1 siRNA dicer substrates (IDT-DNA) were PAI-1 siRNA 1 5′-GCACAAAGAUGGAUGUAAUGCATT-3′ and PAI-1 siRNA 2 5′-UCAUAGAUUUAGGAGCAGAAAUGC-3′. All transfection experiments shown were carried out with PAI-1 siRNA 1. Similar results were obtained with PAI-1 siRNA 2 (data not shown). The sequences of the uPAR siRNA (IDT-DNA) were uPAR siRNA 1 5′-GGUGAAGAAGGGCGUCCAA-3′ and the corresponding control uPAR siRNA 5′-AACCUGCGGGAAGAAGUGG-3′.

qRT-PCR analysis. Total RNA was isolated with the RNeasy mini kit (Qiagen) and reverse transcribed with the iScript cDNA Synthesis kit (Bio-Rad) to generate cDNA. Quantitative PCR was performed using a one-step system (Applied Biosytems, Carlsbad, CA, USA) with sensiMix SYBR (Bioline). The fold difference for various transcripts was calculated by the $2^{-\Delta\Delta CT}$ method[49] using cyclophilin A (PPIA) as the internal control. The following primers were used for qRT-PCR: human PPIA forward (5′-CCAACACAAATGGTTCCCAGT-3′), human PPIA reverse (5′-CCATGGCCTCCACAATATTCA-3′), human PAI-1 forward (5′-ACGTGGTTTTCTCACCCTATGG-3′) and human PAI-1 reverse (5′-CATGCCCTTGTCATCAATCTTG-3′).

Cell proliferation. Transfected cells were plated in 96-well culture plates at a density of 10,000 cells per well in SFM with bFGF (5 ng/ml) for 72 h. When indicated, the cells were treated with bFGF (10 ng ml^{-1}), with or without 16K PRL (50 nM). Proliferation was analyzed 24 h later by measuring BrdU incorporation using the Cell Proliferation ELISA, BrdU (colorimetric; Roche).

Cell migration. A confluent HUVEC monolayer grown in a 48-well tissue culture dish coated with 0.2% gelatin was wounded using a 200-µl tip as described in ref. 50. HUVECs were preincubated with mouse monoclonal anti-LRP (Calbiochem, catalog #438192, 10 µg ml^{-1}), mouse monoclonal anti-uPAR (R&D Systems, clone 62022, catalog #MAB807, 5 µg ml^{-1}) or RAP (Calbiochem, 10 nM) for 1 h and then treated with 50 ng/ml VEGF and with or without 16K PRL (50 nM). Migration of the cells into the wound was recorded 8 h later. Cells transfected with PAI-1 or uPAR siRNA were subjected to the cell migration assay 96 and 72 h after transfection, respectively.

doi:10.1038/nm.3552

NF-κB binding activity. HUVECs were pretreated with a uPAR blocking antibody (R&D Systems, clone 62022, catalog #MAB807, 5 μg ml^{-1}), mouse monoclonal anti-LRP (Calbiochem, catalog #438192, 10 μg ml^{-1}), RAP (Calbiochem, 10 nM) or control IgG (Santa Cruz, catalog #sc-2025), used at the same concentration as the uPAR or LRP antibody) for 1 h and then incubated for 1 h with 16K PRL (50 nM). The p65 DNA-binding activity of NF-κB was quantified by ELISA (EZ Transcription Factor kit NF-κB p65 (Pierce)) according to the manufacturer's instructions using total protein extracts. Protein concentrations were determined by the Bradford method using the BCA protein assay reagent (Pierce). Chemiluminescence was quantified with a luminometer. Cells transfected with PAI-1 or uPAR siRNA were subjected to the NF-κB assay activity assay 96 or 72 h after transfection, respectively.

ERK1/2 phosphorylation. HUVECs were pretreated with a uPAR blocking antibody, mouse monoclonal anti-LRP, RAP or control IgG as described above for 1 h and then treated with 10 ng/ml bFGF and with or without 16K PRL (50 nM) for 15 min. ERK1/2 phosphorylation was detected by western blotting. Protein concentrations were determined by the Bradford method using the BCA protein assay reagent (Pierce). Cells transfected with PAI-1 or uPAR siRNA were subjected to the ERK1/2 phosphorylation assay 96 or 72 h after transfection, respectively.

Immunostaining. Tumor cryosections (5-μm thick) were fixed in acetone at −20 °C and in 80% methanol at 4 °C, saturated with 5% BSA and then incubated with primary antibodies (rat monoclonal anti PECAM-1 (BD Pharmingen, catalog #553370, 1/20) or rabbit polyclonal anti-collagen IV (in-house developed, A.N., 1/100) and monoclonal rat anti-mouse Ki67 (DAKO, catalog #M7248, 1/50)) for 1 h at room temperature. The slides were washed and incubated with a Cy3 goat anti-rat antibody (for PECAM-1, Jackson Immunoresearch, catalog #112-165-003), a Cy3 goat anti-rabbit antibody (for collagen IV, Jackson Immunoresearch, catalog #111-165-144) or an FITC goat anti-rat antibody (for Ki67). After 3 washes in PBS for 10 min, cover slips were placed on the slides in mounting medium (Vector Laboratories Inc.) and the samples were analyzed by fluorescence microscopy. Microvessel size was determined by measuring CD31 staining in each field using NIS-Elements software. The percentage of proliferating tumor cells was determined by counting the number of Ki67 positive cells versus the total number of tumor cells stained by DAPI. At least 500 nuclei were quantified per sample in a total of 7 samples for each condition. The percentage of proliferating cells was determined by staining sections for collagen type IV and Ki67; the number of double-positive cells was counted and expressed as a percentage of the total number of endothelial cells. 100 endothelial cells were analyzed per sample in 7 samples for each condition.

Immunoprecipitation. 300 ng of recombinant 16K PRL was mixed with 5 ng recombinant PAI-1, 1 μl HUVEC-cell-conditioned medium, 250 μl human plasma or 500 μl mouse plasma. For experiments using mice expressing 16K PRL, 50 μl plasma from mice injected with CTL-Ad1 or 16K-Ad adenovirus was collected 5 d after virus injection. The cross-linking agent, DTSSP (Thermo), a nonmembrane permeable cross-linker, was used in all immunoprecipitation experiments to cross-link cell surface proteins on HUVECs, and DSP (Thermo) was used for all other immunoprecipitation experiments. The mixtures were then incubated overnight at 4 °C. Mouse monoclonal anti-PAI-1 antibody (MA-33H1F7, recognizing human and mouse PAI-1, in-house developed, P.J.D.), mouse anti-uPA (American Diagnostica, catalog #3689), mouse anti-tPA MA-51H8 (ref. 51) or the goat polyclonal anti-mouse uPAR (R&D Systems, catalog #AF534) (10 μg ml^{-1}) was then added to each tube and incubated overnight at 4 °C. Fifty microliters of protein A agarose were added to the mix and incubated for 1 h at 4 °C under rotation. After centrifugation for 1 min at 3,000 r.p.m., the supernatants were discarded and the pellets (containing beads) were washed 3 times with PBS. After another centrifugation step, the beads were resuspended in 30 μl 1× β-mercaptoethanol loading buffer and boiled at 100 °C for 5 min. The beads were centrifuged for 5 min at 4 °C and the supernatants subjected to SDS-PAGE (15% acrylamide) for western blot analysis. Latent PAI-1 was produced by incubating recombinant PAI-1 at 37 °C for 48 h.

***In situ* proximity ligation assay.** HUVECs were grown on gelatin-coated glass coverslips. After incubation for 10 min with 16K PRL (50 nM) or for 4 h with 16K PRL (50 nM) and His-tag PAI-1 (2 nM) (for 16K PRL–PAI-1 PLA), the cells were washed with PBS at room temperature and fixed with 4% paraformaldehyde for 15 min, blocked and incubated overnight with 1/100 of the following mouse-rabbit antibody couples: for 16K PRL–PAI-1 PLA, mouse anti His-tag (Invitrogen, catalog #37-2900) and rabbit polyclonal anti-prolactin (Dako, catalog #A0569); for 16K PRL–uPA PLA, mouse anti-mouse uPA (in-house developed, P.J.D.) and rabbit polyclonal anti-prolactin (Dako, catalog #A0569); and for 16K PRL–uPAR PLA, mouse monoclonal anti-prolactin (in-house developed) and rabbit polyclonal anti-uPAR (American Diagnostica, catalog #399R). PLA was performed according to the manufacturer's instructions using the Duolink Detection Kit 563 (Olink Bioscience) with anti-mouse MINUS and anti-rabbit PLUS PLA probes. DAPI stain was added to the probes and the slides were analyzed by fluorescence microscopy.

uPA proteolytic activity. uPA (2 μl at 3 U $μl^{-1}$) was incubated with bovine plasminogen (4 μl at 1 μg $μl^{-1}$) (Sigma) in the presence of PAI-1 (2 μl at 0.5 μg $μl^{-1}$), with or without 16K PRL (5 μl at 1.3 μg $μl^{-1}$). A chromogenic substrate for plasmin (Spectrozyme PL, American Diagnostica) in PBS was added to the mixture in 96-well microtiter plates (final concentration: 0.5 mM) and incubated at room temperature. The release of free *p*-nitroaniline from the chromogenic substrate was measured spectrophotometrically. Plasmin activity was determined as the absorbance at 405 nm.

ELISA for PAI-1 detection. The level of human PAI-1 in mouse plasma was determined using a commercially available ELISA kit for human PAI-1 (American Diagnostica Inc.). Mouse PAI-1 levels in B16F10 tumor extracts were determined by ELISA using the antibody MA-H34G6D10/pAb provided by R. Lijnen (Center for Molecular and Vascular Biology, KU Leuven, Leuven, Belgium).

Clot lysis analysis. Clot lysis was performed as described previously[33] using pooled normal human plasma collected in a citrated tube. Plasma was collected from healthy donors who were informed about the objectives of the study and gave written informed consent. The ethical committee review board of the University Hospital of Liège (comitè d'èthique hospitalo-facultaire universitaire Liège) approved such study on human samples. Recombinant WT PAI-1 (0.5 μM) was preincubated or not for 10 min at 37 °C in the presence or absence of 16K PRL (3 μM). Incubation was performed on 100 μl aliquots at 37 °C in buffer containing 10 mM Tris pH 7.5, 0.01% Tween 20, with final concentrations of recombinant WT PAI-1 (0.05 μM), 16K PRL (0.3 μM), plasma (24% V/V), tPA (240 μM) and $CaCl_2$ (10 mM). Clot formation and dissolution were monitored at room temperature by measuring the turbidity at 405 nm at 5-min intervals.

Adenovirus vectors. 16K-Ad is a defective recombinant adenovirus vector (with E1 and E3 deleted) encoding a secreted polypeptide consisting of the first 139 amino acids of human PRL. This adenovirus vector was constructed as described previously[7] with the help of the Adeno-X expression system (BD Biosciences). CTL-Ad1, the control for 16K-Ad1, previously called Null-Ad[7], carries an empty expression cassette. A recombinant adenovirus vector bearing WT human PAI-1 (PAI-1-Ad2) and its control adenovirus (CTL-Ad2) were generated as described[21] (previously called AdCMVPAI-1 and AddRR5, respectively).

Mouse tumor models. Homozygous PAI-1–deficient mice and their WT littermates (genetic background 87% C57BL/6, 13% 129S6)[52], PAI-1–deficient Rag–deficient mice and their WT Rag–deficient littermates[53], uPA-deficient mice and their WT littermates (genetic background 75% C57BL/6, 25% 129S6)[54] and the corresponding WT mice of either sex were used throughout the study. Briefly, subconfluent B16F10 cells or 4T1 cells were trypsinized, washed and resuspended in PBS. B16F10 cells (1×10^5 cells in 50 μl PBS) were injected subcutaneously into the right flank of each mouse (7 mice per group). 4T1 cells (2×10^5 cells in 50 μl PBS) were injected orthotopically into the left mouse mammary gland of PAI-1–deficient Rag–deficient mice or their corresponding

controls (8 female mice per group). 16K-Ad or CTL-Ad1 was injected intravenously 2 d before the injection of tumor cells. Five days after vector injections, the level of 16K PRL in plasma of mice injected was 30.99 ± 9.6 μg ml^{-1} ($n = 3$) as determined by ELISA (R&D system). To maintain 16K PRL expression, a second injection of 16K-Ad or CTL-Ad was administered 8 d after the first. PAI-1-Ad or CTL-Ad2 was injected 1 d after each 16K PRL adenovirus injection. Virus dose was 1×10^9 PFU per injection in all cases. Tumor growth of B16F10 cells was assessed by measuring the length and width of each tumor every 1 to 2 d and calculating tumor volume by means of the formula length × $width^2 \times 0.5$. Only palpable tumors were included for the analysis of tumor growth. Eighteen to twenty days after tumor cell injection, mice were euthanized and their tumors harvested. For the 4T1 tumor model, tumor weight was determined at 15 d after tumor injection. The animal experiment protocol used was approved by the Institutional Ethics Committee of the University of Liège.

Keratinocyte transplantation model. Malignant mouse keratinocytes (BD VII cells[13]) (2×10^5) were plated on collagen gels (4 mg ml^{-1} type I collagen isolated from rat tail tendons) inserted in Teflon rings (Renner GmbH, Germany) and maintained in culture for 1 d. The cell-coated collagen gels were covered with a silicone transplantation chamber (Renner GmbH) and implanted *in toto* onto the dorsal muscle fascia of mice as described previously[22]. Two weeks later, transplants were resected, embedded in Tissue Tek (Miles Laboratories, Inc.) and frozen in liquid nitrogen for cryostat sectioning. Immunostaining was performed with FITC-conjugated anti-keratin (guinea pig polyclonal antibody, Sigma, catalog # K4252 1/20) and anti-type IV collagen (rabbit polyclonal antibody, in-house developed, A.N., 1/100). Quantification of tumor invasion and angiogenesis was performed by morphometric measurements using NIS-Elements software. In this model, the collagen gel is progressively replaced by vascularized granulation tissue, upon which malignant cells invade downwards, so that after two weeks, the entire collagen gel is replaced by malignant and host cells[22,24]. The yellow downward-pointing arrow (**Fig. 3a**) denotes the distance over which the tumor cells invaded the collagen gel and host tissue (referred to as the invasion parameter 'i'). Vascularization of the transplanted tumor was analyzed by measuring the distance over which host vessels grew into the collagen gel and tumor (referred to as the angiogenesis parameter 'a'). In the case that host vessels invaded all the way up into the tumor tissue itself (as in control conditions in WT mice; **Fig. 3a**), we measured the distance over which the host vessels migrated, starting from the hypodermis, into the tumor tissue (denoted by upward-pointing white arrow (**Fig. 3a**) and expressed as 'positive' distance in **Fig. 3c**). However, when WT mice received 16K-Ad1, the host vessels grew over some distance into the collagen gel but failed to grow all the way up into the tumor tissue (**Fig. 3a**). In this case, the vascularization defect was quantified by measuring the length of the remaining nonvascularized gel, starting from the tumor (denoted by the downward-pointing white arrow (**Fig. 3a**) and expressed as 'negative' distance in **Fig. 3c**). For each parameter ('i' and 'a'), the average value of 6–8 measurements per tumor was used, and mean values for 6 tumors are reported. The animal experiment protocol used was approved by the Institutional Ethics Committee of the University of Liège.

Mouse retinal angiogenesis model. To analyze postnatal angiogenesis in the mouse retina, neonatal mice from either sex were injected intraocularly at postnatal day (P) 1 with 85 nmol/eye of recombinant 16K prolactin or vehicle and sacrificed at P4.5. The eyes were fixed in 4% paraformaldehyde in PBS for 45 min; the retinas were dissected, post-fixed and stained with Isolectin B4 (Vector laboratories, catalog # B-1205) before being flat-mounted as previously described[25]. The retinal radius (from the optic nerve to the edge of the retina) and the vascular radius (from the optic nerve to the vascular front) of each petal of the flat-mounted retina were measured. The value for each retina was calculated as the mean of the radii for all petals. Vascular coverage was calculated as the ratio between vascular radius and retinal radius. Three to five neonates were included in each treatment group. The animal experiment protocol used was approved by the Institutional Ethics Committee of the University of Liège.

Matrigel plug assay. Matrigel plug implantation was performed as previously described[55]. Matrigel (BD Biosciences), supplemented with 250 ng/ml fibroblast growth factor-2 (FGF-2) and 0.0025 U ml^{-1} heparin (Sigma-Aldrich, Belgium), was incubated with 16K PRL (200 nM) or with buffer. 500 μl of Matrigel was implanted subcutaneously into the right and left flanks of C57BL/6 mice of either sex under anesthesia. For experiments with WT and PAI-1–deficient mice, Matrigel without added 16K PRL was used, and the mice were treated with 16K PRL (16K-Ad1) or CTL (CTL-Ad1) adenovirus on the same day as Matrigel implantation. After 7 or 15 d, the plugs were dissected from the mice and their weight was determined. The Matrigel plugs were ground in the presence of dispase solution. The concentration of hemoglobin in the supernatant was then determined directly by absorbance at 405 nm and compared with a standard curve of purified hemoglobin (Sigma). The animal experiment protocol used was approved by the Institutional Ethics Committee of the University of Liège.

Mouse carotid artery blood flow restoration model. Mice (7 to 9 weeks old, males) were anesthetized by intraperitoneal injection of 125 mg kg^{-1} ketamine and 12.5 mg kg^{-1} xylazine in NaCl 0.9%. A Doppler flow probe (MA 0.5 PSB, Transonic Systems) was placed on the left carotid artery and blood flow was recorded. Carotid artery injury was induced by placing a filter paper (1 × 2 mm, Whatman GmbH, Germany) saturated with 10% FeCl 3 for 3 min (Sigma-Aldrich, Belgium) on the left carotid artery, causing occlusion and blood flow arrest within about 5 min. Five minutes before injury, vehicle (150 μl) or recombinant 16K PRL (1.5 mg kg^{-1}) was injected via a catheter in the tail vein. Ten minutes after occlusion, unfractionated porcine heparin (200 U kg^{-1}) was administered followed by a continuous heparin infusion (70 U kg^{-1} h^{-1}). Ten minutes later, a continuous tPA (100 μg kg^{-1} min^{-1}) (Actilyse, Boehringer Ingelheim, Belgium) and heparin infusion (70 U kg^{-1} h^{-1}) was started. The time to reperfusion, defined as the interval between initiation of tPA administration and return of carotid flow to 50% of baseline, was recorded. Carotid blood flow was monitored with a Doppler flow probe for 90 min after occlusion. The animal experiment protocol used was approved by the Institutional Ethics Committee of the University of Liège.

Mouse thromboembolism model. BALB/c CjRj mice (Janvier Labs, France) (body weight 15–18 g) were used under continuous anesthesia with ketamine/xylazine throughout the entirety of the experiment. Recombinant 16K PRL (1 mg kg^{-1}) was administered via retro-orbital vein injection. Five minutes later, a suboptimal concentration of tPA (0.1 mg kg^{-1}) was injected i.v., immediately followed by i.v. injection of thromboplastin (Dade Innovin, 3.3 μg kg^{-1}, Siemens) to evoke thromboembolism[56]. Mice were evaluated after 15 min for survival. For the experiment with adenovirus vectors, mice were i.v. injected with 1×10^9 PFU of 16K PRL adenovirus (16K-Ad1) or its corresponding control (CTL-Ad1). Five days after the injection, a suboptimal concentration of tPA (0.1 mg kg^{-1}) was injected i.v., immediately followed by i.v. injection of thromboplastin. Thromboplastin dose was 3.3 μg kg^{-1} for BALB/c mice and 0.165 μg kg^{-1} for PAI-1 KO mice and their WT littermates (genetic background 87% C57BL/6: 13% 129S6), which showed higher sensitivity to the thromboplastin-induced pulmonary embolism model. Mice from either sex were used. For lung histology, lungs were removed 15 min after injection of thromboplastin and fixed in 4% formaldehyde. Cryosections were stained with hematoxylin and eosin. In all cases, five fields were examined and identifiable thrombus-occluded vessels were counted in each field. The animal experiment protocol used was approved by the Institutional Ethics Committee of the University of Liège.

Statistical analyses. All data are expressed as mean ± s.e.m., unless otherwise indicated. All *in vitro* experiments were performed in triplicate and were repeated at least 3 times unless otherwise indicated. The *in vitro* migration, proliferation and NF-κB activity data were calculated relative to the controls in each experiment, and general linear model univariate analysis was used to determine differences between treatment groups, using experiment as covariate. Fisher's exact test was used to determine the difference between groups in the blood flow restoration and pulmonary embolism survival experiments. For the 4T1 tumor experiment, data were analyzed using nonparametric Mann-Whitney *U* test. All other data were analyzed with the Student's *t*-test. Statistical significance was set at $P < 0.05$.

doi:10.1038/nm.3552

45. Gils, A., Knockaert, I. & Declerck, P.J. Substrate behavior of plasminogen activator inhibitor-1 is not associated with a lack of insertion of the reactive site loop. *Biochemistry* **35**, 7474–7481 (1996).
46. Thijssen, V.L. *et al.* Galectin-1 is essential in tumor angiogenesis and is a target for antiangiogenesis therapy. *Proc. Natl. Acad. Sci. USA* **103**, 15975–15980 (2006).
47. Jaffe, E.A., Nachman, R.L., Becker, C.G. & Minick, C.R. Culture of human endothelial cells derived from umbilical veins. Identification by morphologic and immunologic criteria. *J. Clin. Invest.* **52**, 2745–2756 (1973).
48. Fusenig, N.E., Amer, S.M., Boukamp, P. & Worst, P.K. Characteristics of chemically transformed mouse epidermal cells *in vitro* and *in vivo*. *Bull. Cancer* **65**, 271–279 (1978).
49. Livak, K.J. & Schmittgen, T.D. Analysis of relative gene expression data using real-time quantitative PCR and the $2^{-\Delta\Delta C_t}$) Method. *Methods* **25**, 402–408 (2001).
50. Sabatel, C. *et al.* MicroRNA-21 exhibits antiangiogenic function by targeting RhoB expression in endothelial cells. *PLoS ONE* **6**, e16979 (2011).
51. Ngo, T.H., Debrock, S. & Declerck, P.J. Identification of functional synergism between monoclonal antibodies. Application to the enhancement of plasminogen activator inhibitor-1 neutralizing effects. *FEBS Lett.* **416**, 373–376 (1997).
52. Carmeliet, P. *et al.* Plasminogen activator inhibitor-1 gene-deficient mice. I. Generation by homologous recombination and characterization. *J. Clin. Invest.* **92**, 2746–2755 (1993).
53. Bajou, K. *et al.* Plasminogen activator inhibitor-1 protects endothelial cells from FasL-mediated apoptosis. *Cancer Cell* **14**, 324–334 (2008).
54. Carmeliet, P. *et al.* Physiological consequences of loss of plasminogen activator gene function in mice. *Nature* **368**, 419–424 (1994).
55. Passaniti, A. *et al.* A simple, quantitative method for assessing angiogenesis and antiangiogenic agents using reconstituted basement membrane, heparin, and fibroblast growth factor. *Lab. Invest.* **67**, 519–528 (1992).
56. Vercauteren, E. *et al.* Evaluation of the profibrinolytic properties of an anti-TAFI monoclonal antibody in a mouse thromboembolism model. *Blood* **117**, 4615–4622 (2011).